Optimal Synthesis of Conically Shaped Dielectric Elastomer Linear Actuators: Design Methodology and Experimental Validation

Giovanni Berselli, Rocco Vertechy, Gabriele Vassura, and Vincenzo Parenti-Castelli

***Abstract*—An analytical model and an operational procedure are presented, which make it possible to optimize conically shaped dielectric–elastomer linear actuators for known materials and desired force/stroke requirements. The actuators are obtained by coupling a dielectric elastomer film with a compliant frame which is sized by means of a pseudorigid body model. Depending on the frame design, the actuators can work monodirectionally or bidirectionally. Simulation and experimental results are provided which demonstrate the efficacy of the proposed design procedure and show that well-behaved conically shaped actuators can be conceived and produced.**

***Index Terms*—Compliant mechanisms, dielectric elastomer actuators, optimal design.**

I. Introduction

AMONG the class of materials known as electroactive polymers, dielectric elastomers (DEs) represent one of the best materials that can be used for the development of solid-state linear actuators. DE-based linear actuators offer high power density and good efficiencies combined with relatively low weight and extremely low costs.

For actuation usage, DE can be shaped in thin films which are first prestretched and then coated with compliant electrodes on both sides to form an electrically deformable film (EDF). The term EDF simply identifies a dielectric, hyperviscoelastic, and incompressible isotropic membrane (the DE) placed between two compliant electrodes [1]–[3]. Activation of the EDF via the placement of large electric potential differences (hereafter also called voltages) between the electrodes can induce film area expansions, and thus, points' displacements which can be used to produce useful mechanical work (whenever forces are applied to such points).

Manuscript received April 1, 2010; revised September 10, 2010; accepted October 15, 2010. Date of publication December 20, 2010; date of current version January 12, 2011. Recommended by Guest Editor P. Sommer-Larsen. This work was supported in part by the Italian Ministero dell'Istruzione, dell'Università e della Ricerca with the PRIN20082008FS39YF (*New Actuators for Advanced Systems of Manipulation and Haptic Interaction*) and in part by INTERMECH-MECTRON, Mechatronics Laboratory of Regione Emilia Romagna.

G. Berselli, G. Vassura, and V. Parenti-Castelli are with the Dipartimento di Ingegneria delle Costruzioni Meccaniche, Nucleari, Aeronautiche e di Metallurgia, Mechanical Engineering Department, University of Bologna, 40136 Bologna, Italy (e-mail: giovanni.berselli@unibo.it; gabriele.vassura@unibo.it; vincenzo.parenti@unibo.it).

R. Vertechy is with Perceptual Robotics Laboratory (PERCRO), Scuola Superiore Sant'Anna, 56025 Pontedera, Italy (e-mail: r.vertechy@sssup.it).

Color versions of one or more of the figures in this paper are available online at http://ieeexplore.ieee.org.

Digital Object Identifier 10.1109/TMECH.2010.2090664

Different kinds of DE-based actuators with various shapes have been proposed in the literature (see, for instance, in [4] for details) some of which can be obtained by first uniformly prestretching the EDF (that is often necessary since the film has negligible flexural rigidity) and then by coupling some segment of its boundary to some portion of a flexible supporting frame, either an elastic structural element (for instance, a helical spring) or a compliant mechanism (for instance, a four-bar mechanism with elastic revolute joints) [5]–[15].

The flexible frame can be specifically designed to modify the overall actuator stiffness which heavily depends on the EDF elastic properties. In particular, depending on the frame design, the actuator can work monodirectionally (see, for instance, in [14]) or bidirectionally (see, for instance, in [15]) as long as the frame stiffness can be used to provide a restoring force that brings back the actuator to a reference initial position when the EDF is deactivated. Furthermore, particular frame designs enable obtaining a constant available thrust over a given range of motion.

Actuators with constant available thrust (usually referred to as *constant output force actuators*) are typically desirable since they possess uniform behavior, enable optimal use of the available output work, and are easy to control [16]–[18]. For instance, note that constant output force actuators are capable of applying a given desired force even in the presence of small system deflections or positioning errors, and therefore, minimize the required controller effort. Such devices are needed in haptics, mobile robots, and systems for delicate part handling and material machining/testing [17], [18].

Much work has been dedicated to the design of constant force drive units. These include either the conception of traditional electromagnetic, hydraulic, and pneumatic actuators directly having constant force–length (FL) curves [19], or the development of special mechanical transmissions [17]–[19] and of complex control algorithms [20], [21] to adjust the output force of actuators (such as those based on piezoelectric and shape-memory materials) inherently featuring nonconstant FL curves. Practical examples of DE-based linear actuators capable of providing a nearly constant force have been proposed in [13], [22], and [23] concerning EDFs which are shaped as lozenges and in [14] concerning EDFs which are shaped as rectangles. The authors themselves remarked both the advantages and the critical aspects of such designs.

Similarly to the aforementioned solutions, an actuator morphology that has shown promising properties in various applications (e.g., Braille cells [24], lightweight robots [25], and

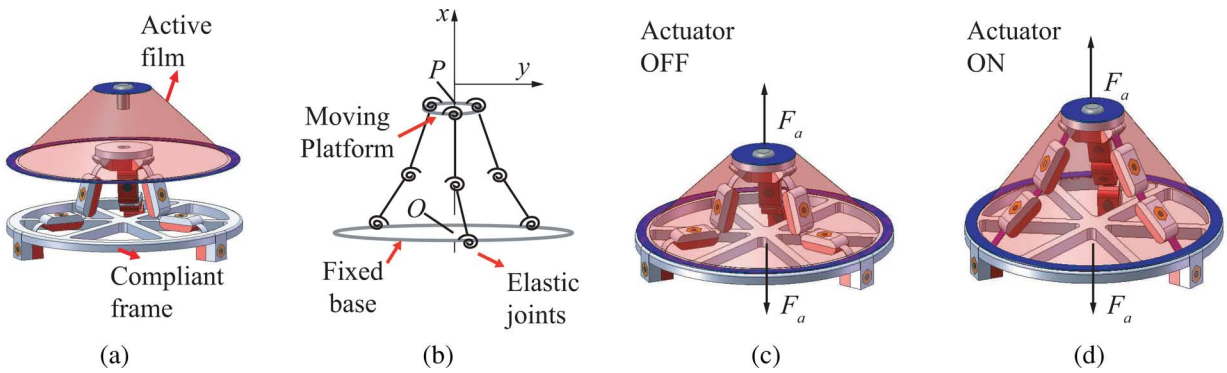

Fig. 1. Concept behind the proposed solution. (a) Assembly exploded view, (b) compliant frame schematic, CAD model in (c) deactivated and (d) activated states.

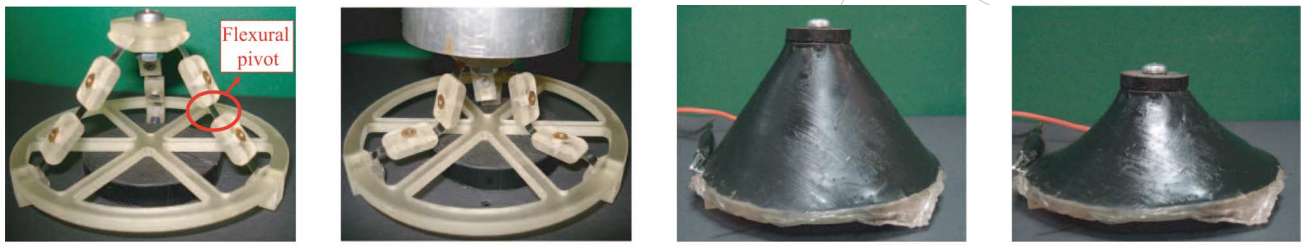

Fig. 2. Actuator prototype. Frame prototype in (a) undeflected condition and (b) under constant external load application, actuator in (c) deactivated and (d) activated states.

medical [26] and haptic devices [27]) is the conically shaped DE linear actuator [5]–[7], [28], [29] which, however, normally supplies an available thrust that heavily varies along its stroke (see, for instance, in [28] and [29] for experimental results). This behavior is hereafter modified by coupling the conical EDF with a compliant frame designed as an overconstrained parallel mechanism having three equal legs articulated via three revolute joints with parallel axes. The CAD exploded view of the actuator is shown in Fig. 1(a), the schematic (pseudorigid model [30]) of the compliant frame is shown in Fig. 1(b) whereas the actuator CAD models showing the coupling between the EDF and the frame are shown in Fig. 1(c) and (d). With reference to Fig. 1(b), displacements of the moving platform along the radial, y, direction (or, alternatively, rotations) are prevented by the parallel tripod architecture. The revolute joints of the parallel mechanism are designed as "Small-length Flexural Pivots" [30], [31] i.e. as short flexible segments whose resistance to deflection is modeled using a torsional spring. The frame prototype is shown in Fig. 2(a) (undeflected condition) and in Fig. 2(b) (moving platform loaded with a constant load acting in the axial, x, direction). The overall actuator prototype is depicted in Fig. 2(c) (actuator deactivated state) and in Fig. 2(d) (actuator activated state).

In the following, a novel procedure is proposed for the optimal design of such conically shaped DE-based linear actuators. In particular, on the basis of simplified, but yet accurate, design equations, a methodology is presented which makes it possible to improve the actuator force/stroke performance. Then, case study simulation and experimental results are reported, which highlight both the efficiency of the procedure and the improved performances of an optimized conically shaped actuator prototype.

II. Compliant Frame Effect on the Actuator Performance

Recalling general design guidelines reported in [14], it can be stated that the EDF deformation produces a variation of the actuator length $x = |(P - O)|$, where P and O are, for instance, two points of the actuator lying on the EDF axis of symmetry [Fig. 1(b)], and a force having the same direction of vector $\overline{OP}$[1] that can be supplied to an external user. This force, called the actuator available thrust, $F_a(V, x, \dot{x})$, is generally given by the sum of two contributions, $F_f(V, x, \dot{x})$ and $F_s(x)$

$$F_a(V, x, \dot{x}) = F_f(V, x, \dot{x}) + F_s(x) \tag{1}$$

where F_a is the available thrust, x is the actuator length ($\dot{x}$ being its time derivative), V is the voltage applied to the EDF, F_s is the frame reaction force (due to the frame's own stiffness and function of the actual actuator configuration), and F_f is the EDF force, i.e, the resultant force in the direction of actuation due to the stress field arising in the EDF. This field depends on the amount of given prestretch, on the applied voltage, and on the actuator configuration/velocity. According to a 1-D lumped parameter model, the EDF behaves as a nonlinear spring–damper (the spring having stiffness $K_f = dF_f/dx$ and being subjected to tension at all times) whereas the flexible frame behaves like

[1]The direction of vector $\overline{OP}$ will be referred to as the direction of actuation.

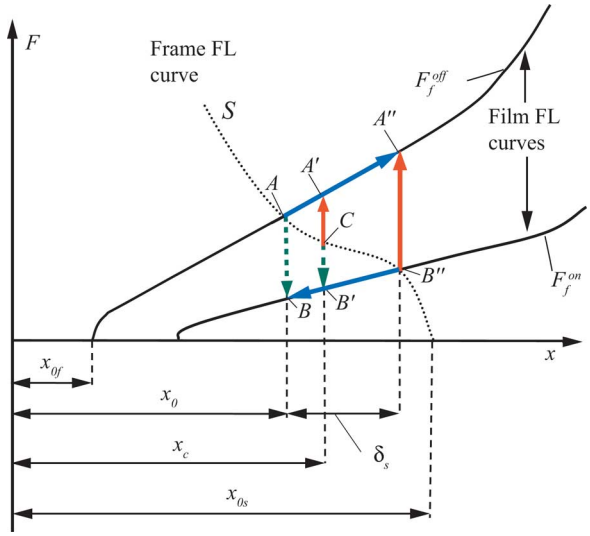

Fig. 3. FL curves qualitatively showing the moduli of F_f and F_s.

a nonlinear compression spring (with stiffness $K_s = dF_s/dx$) coupled in parallel with the EDF. Conventionally, F_a is the force that an external user supplies to the actuator.

Fig. 3 shows qualitative diagrams of FL curves concerning internal forces F_f and F_s, adopting a representation methodology widely used in the study of interacting elastic structures where the moduli of the forces are shown. Note that the time-dependent behavior of the DE, such as rate-dependent hardening, creep, stress relaxation, and hysteresis, is neglected in these plots. In the following, the terms "OFF-state" and "ON-state" will identify every actuator working condition where $V = 0$ and $V \neq 0$, respectively. Therefore, the *continuous* curve F_f^{OFF} represents the film force F_f in the OFF-state ($K_f^{\mathrm{OFF}} = dF_f^{\mathrm{OFF}}/dx$ being its stiffness) whereas the *dotted* curve S represents the modulus of the reaction force F_s of a possible frame.

In the OFF-state, after the coupling of the prestretched film and the precompressed frame, the achieved equilibrium position is represented by point A. In this condition (no applied load and no applied voltage), the actuator initial length is x_0. The displacements imposed on the 1-D springs representing the film and the frame are given, respectively, by $|x_0 - x_{0f}|$ and $|x_{0s} - x_0|$, where x_{0f} is the free length of the EDF and x_{0s} is free length of the frame. Point A is taken as the reference point for the measurement of the actuator stroke δ. On the other hand, the *continuous* curve F_f^{ON} represents the relationship between the film force F_f and the actuator length ($K_f^{\mathrm{ON}} = dF_f^{\mathrm{ON}}/dx$ being its stiffness), in the case of EDF activation under constant voltage (let us consider the maximum actuation voltage $V = V_{\max}$). Point B represents the new value of F_f upon a step voltage rise, starting from point A. The distance between points A and B symbolizes the available thrust F_a. In this condition, $|F_f| < |F_s|$ and the actuator output can move outward (i.e. increase its own length). If the actuator output is free to move (no external load), the actuator can reach a new equilibrium position represented by point B''. The term δ_s represents the maximum stroke obtainable with a frame characterized by an FL profile like curve S.

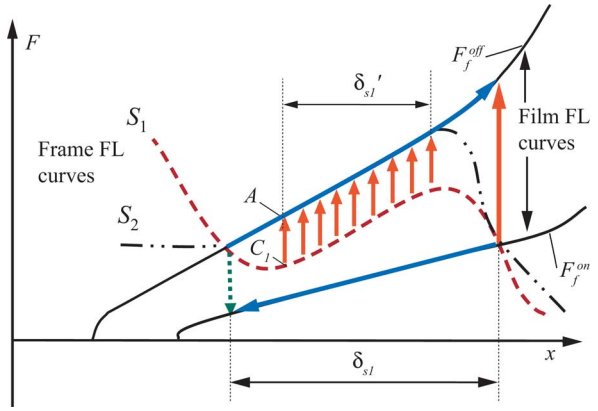

Fig. 4. FL curves qualitatively showing the moduli of F_f and F_s and the "negative stiffness" effect.

In any intermediate position defined by x, points C and B' represent, respectively, forces F_s and F_f^{ON}; in this condition, the available thrust is equal to the distance $\overline{B'C}$. If, at any point along the stroke, the excitation voltage is suddenly removed, the force acting on the film abruptly passes from point B' to point A', thus obtaining $|F_f| > |F_s|$and an available thrust acting in the opposite direction with absolute value equal to the distance $\overline{A'C}$. It can be seen that, in general, F_a varies along the stroke δ, both outward and backward, whereas a constant thrust would be preferable. However, the force profiles of F_a in the ON- and OFF-states (F_a^{ON} and F_a^{OFF}, respectively) can be modified by working on the frame design depending on the application requirements. Assuming the EDF electromechanical characteristics as given, let us suppose that the EDF is coupled with a compliant mechanism whose elastic reaction force increases in modulus as the actuator length $x$increases. In a 1-D model, such a frame can be conceived as a negative stiffness spring acting in parallel with the EDF. In general, this behavior is exhibited by mechanisms characterized by unstable equilibrium positions (UEPs) along their motion (for instance, bistable elements having an UEP between two stable equilibrium positions (SEPs)) (see, for instance, in [11]). If this negative stiffness perfectly matches the EDF stiffness, a constant output force can be obtained.

As an example, let us first consider a frame FL profile represented by curve S_1 (Fig. 4); it can be seen that, for a consistent part of the stroke (namely δ_{s1}'), F_a maintains a constant value, F_a^{OFF}, equal to the distance $\overline{AC_1}$ as the actuator is in its OFF-state. In this case, the overall actuator stroke is increased to δ_{s1}. If needed, the stroke can be limited by means of mechanical stops (for instance, in order to prevent its functioning in regions where F_a^{OFF} is not constant). The ON-state available thrust, F_a^{ON}, is maximized by choosing a frame FL curve like the one depicted by curve S_2 in Fig. 4, that is, $F_a^{\mathrm{OFF}} = 0$ for a given range of motion. Differently from the solution where curve S_1 is employed (double-acting actuator), a null thrust in the OFF-state results in an actuator capable of working in one direction only (single-acting actuator). In such a case, for applications requiring control via bidirectional forces, two identical actuators must be employed in an agonistic–antagonistic configuration.

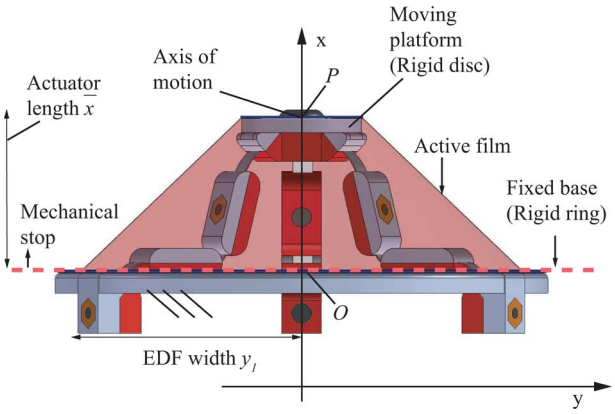

Fig. 5. Actuator configuration under no load and no voltage.

Note that, as long as the film FL curves F_f^{OFF} and F_f^{ON} are generally not parallel, a constant force in the OFF-state does not guarantee a constant force in the ON-state. In particular, three principal cases can be outlined:

1) Constant force in the OFF-state: $F_s = -F_f^{\mathrm{OFF}} + a_1$, resulting in a single-acting actuator if $a_1 \leq 0$.
2) Constant force in the ON-state: $F_s = -F_f^{\mathrm{ON}} + a_2$, resulting in a single-acting actuator if $a_2 \geq 0$.
3) Minimization of the available thrust variation along the stroke: $F_s = -(F_f^{\mathrm{OFF}} + F_f^{\mathrm{ON}})/2$.

III. Proposed Solution Concept

The concept behind the proposed solution is shown in Figs. 1, 2, and 5.

As said, the compliant frame is designed as an overconstrained parallel mechanism featuring a moving platform (the rigid disk), a fixed base (the rigid ring), and three equal legs articulated via three revolute elastic joints with parallel axes. The frame supports the EDF [via a rigid ring and a rigid disk (Fig. 5)] and, at the same time, provides the desired FL profile. Thanks to the mechanism symmetry and to the adoption of elastic joints, each leg behaves as a fully compliant slider–crank mechanism (CSCM) whose pseudorigid body model (PRBM) [30] is depicted in Fig. 6(a). Referring to Fig. 6(a), r_1 and r_2 are the crank and the connecting rod lengths, respectively, e is the slider–crank mechanism eccentricity, x is the mechanism length (i.e., the distance between the points O and P), K_1, K_2, K_3 are the spring constants of the compliant joints [30], ϑ_1 and ϑ_3 are the crank angle and connecting rod angular positions measured with respect to the actuator direction of motion ($\vartheta_2 = \vartheta_3 - \vartheta_1$), and ϑ_{10}, ϑ_{20}, ϑ_{30} are the undeflected angular positions of the flexural pivots ($\vartheta_{20} = \vartheta_{30} - \vartheta_{10}$).

Let us define the force F_s' as the CSCM reaction force due to its own stiffness, that is a function of the actual mechanism configuration. Invoking the principle of the superimposition of the effects, the force F_s' is given by

$$F_s' = F_1 + F_2 + F_3 \tag{2}$$

where the forces F_1, F_2 and F_3 are due to the deflection of the torsional springs with stiffness K_1, K_2 and K_3 respectively. Let us consider separately the contribution of each stiffness K_1, K_2 and K_3.

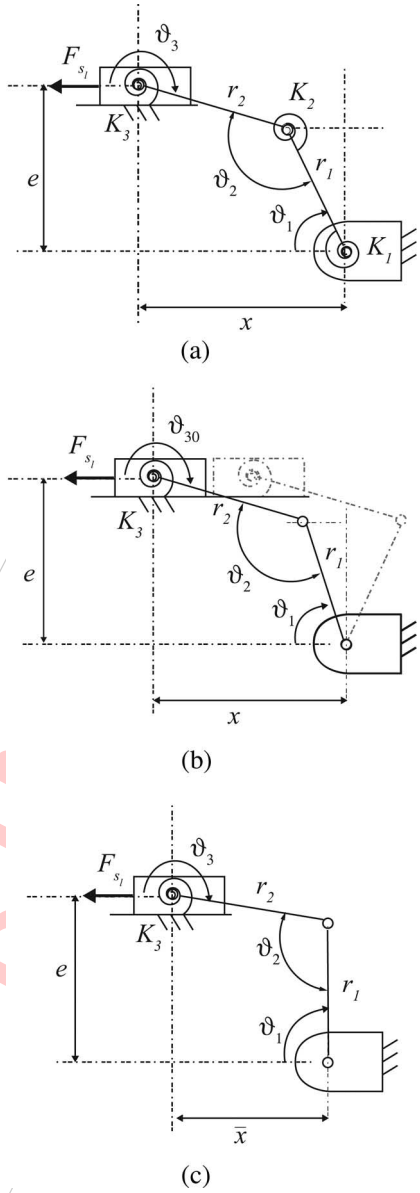

Fig. 6. Slider-crank compliant mechanism (CSCM), pseudorigid-body model. (a) CSCM: uninflected (stable) position. (b) Reduced CSCM: first (continuous black line) and second (dashed red lines) stable positions. (c) Reduced CSCM: unstable position.

At first, neglect the contribution of torsional springs with stiffnesses K_1 and K_2, such that $F_s' = F_3$. In such a situation, the resulting mechanism (hereafter referred to as "reduced" CSCM) is depicted in Fig. 6(b), where the torsional spring with stiffness K_3 is represented in its undeflected positions. As long as the spring K_3 can reach an uninflected position for two mechanism configurations, the reduced CSCM is bi-stable (the first SEP being depicted as a continuous black line, the second SEP being depicted as a dashed red line). A UEP is reached when the rocker arm is perpendicular to the slider direction of motion [Fig. 6(c)]. Let us now neglect the contribution of the torsional spring with stiffness K_3, and therefore, consider the contribution of the

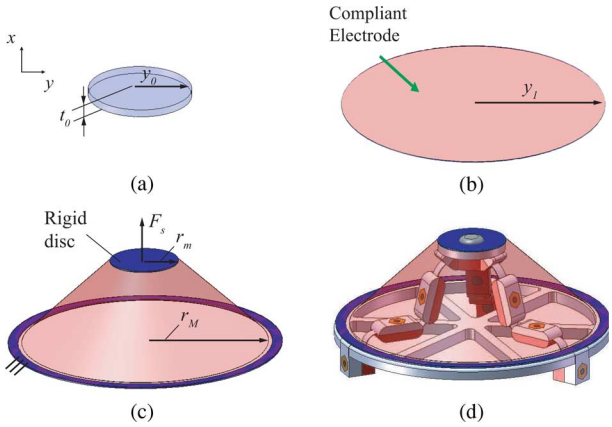

Fig. 7. Production steps for the manufacture of the actuator. (a) Unloaded DE. (b) Equibiaxially prestretched DE with electrodes (EDF). (c) Application of external load to the ED. (d) Final actuator (EDF + compressed frame) equilibrium position.

forces F_1 and F_2 only. Define $F_{12} = F_1 + F_2$. The resulting mechanism is a possible topology of a compliant mechanism that can supply a nearly constant force if suitably dimensioned [32].

That is, the CSCM can be used to tailor the actuator-available thrust by altering its stiffness (by means of F_3) and altering the thrust initial value $F_a(x_0, V)$ (by means of F_{12}).

Regarding actuator manufacturing, a circular EDF with initial radius equalling y_0 [Fig. 7(a)] is first subjected to an equibiaxial prestretch up to a final radius denoted as y_1. Then, it is coated with compliant electrodes on both sides to form an EDF [Fig. 7(b)]. Finally, the application of an external force in the x direction (which is supplied by the platform of the compliant frame) causes the EDF to gain a conical shape [Fig. 7(c)]. Note that, as it can be seen from Fig. 2(c) and (d), the EDF is, in fact, deformed into an out-of-plane, axisymmetric shape which approximates a right circular cone as the actuation voltage is increased. The fixed base can provide a mechanical stop that prevents the actuator from operating in regions below the UEP, i.e., such that $x < \bar{x}$ (Fig. 5). Both EDF and frame need to be suitably dimensioned for the specific application. In the following, a mathematical model of the overall actuator behavior is described in detail.

IV. Model Development

A. Electromechanical Behavior of Conically Shaped Dielecric Elastomer Films

The EDF used in this paper for the experimental validation of the proposed design methodology is a membrane of an acrylic elastomer (VHB-4905) whereas the compliant electrodes are made with a conductive grease. In essence, EDFs are viscoelastic capacitors that deform and/or generate forces in response to mechanical and electrical loads/constraints. The behavior of EDFs with general geometry can be rather complicated, especially whenever they undergo nonuniform large deformations, which may require coupled nonlinear electromechanical numerical models for a truthful representation. The typical experimental tensile response of a conically shaped EDF specimen

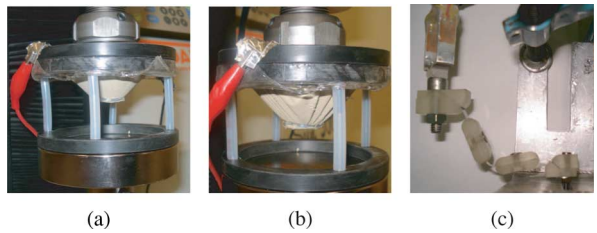

(a) (b) (c)

Fig. 8. Experimental setup for the determination of (a) EDF force F_f and (c) frame force F_s. EDF wrinkling under (b) high actuation voltages.

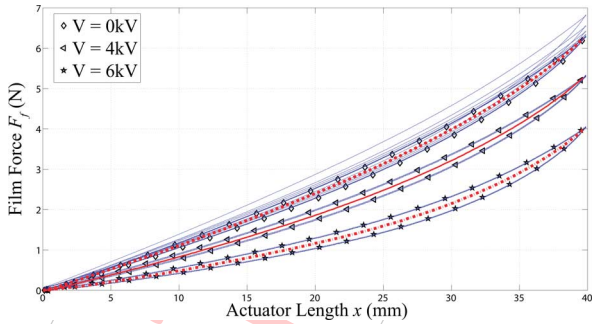

Fig. 9. Experimental FL curve of a conically shaped EDF specimen subjected to mechanical and electrical loading–unloading cycles.

subjected to mechanical and electrical loading–unloading cycles is shown in Fig. 9.

The specimen consisted of a virgin circular acrylic DE with initial radius and thickness equalling $y_0 = 10$ mm and $t_0 = 1.5$ mm, which is prestretched up to a radius of $y_1 = 40$ mm coated with conductive grease and glued to a rigid ring with internal radius $r_M = y_1$ and to a concentric rigid disk with external radius $r_m = 12$ mm [refer to Fig. 7(c)]. The specimen was placed in a tensile stage [Fig. 8(a)] which, by keeping the ring fixed and moving the disk along its axial, x direction, enabled to acquire the film FL curves. The setup is configured such that the x positive direction is opposed to gravity. The deflection of the EDF due to its own weight is reasonably neglected. The tensile test consisted in cyclically displacing the disk between the length $x = 0$ and $x = 40$ mm at a constant velocity of 1 mm/s, while the EDF electrodes were subjected to an electric potential difference (electrical activation) equalling $V = 0$ kV for the first eight cycles, $V = 4$ kV for the subsequent three cycles and $V = 6$ kV for the last three cycles. During the test, the specimen length and the tensile force were measured with an accuracy of less than 10 μm and 0.01 N, respectively; the room temperature was 21 °C. Fig. 9 highlights that the electromechanical response of typical conically shaped EDFs feature exhibits:

1) a reduction in stress (stress softening) at a given strain on each successive loading, which is largest in the first loading–unloading cycle, becomes rather negligible after about three cycles, and is rather insensitive to EDF electrical activation;
2) sensible difference between the loading and unloading forces (hysteresis) corresponding to the same deformation level whose magnitude is rather insensitive to EDF electrical activation.

Removing rigid ring and disk highlights that the EDF remains affected by a residual stretch (permanent set) λ_r, which is mostly generated during the initial prestretch and the first three loading–unloading cycles (notice, however, that this permanent set slowly decreases in time and essentially disappears after a sufficiently large period of annealing whenever the film is left in an unloaded condition). That is, after about three preconditioning loading–unloading cycles (blue solid line in Fig. 9), the electromechanical response of the acrylic conically shaped EDF becomes essentially repeatable irrespective of the imposed electric potential difference (lozenge-, triangle- and star-marked dark lines in Fig. 9 for the activation potentials $V = 0$ kV, $V = 4$ kV, and $V = 6$ kV, respectively). The hysteretic response of the tested acrylic conically shaped EDF is a rate-dependent effect which tends to disappear for very slow deformation rates. The stabilized equilibrium behavior (hereafter referred to as experimental stabilized equilibrium curve), which is related to infinitely slow deformation rates [33], is reported in Fig. 9 with dashed, continuous, and dash-dotted red lines for the activation potentials $V = 0$ kV, $V = 4$ kV, and $V = 6$ kV, respectively (these paths have been determined according to the procedure described by Bergstrom and Boyce [33]).

B. Electromechanical Analytical Model for Conically Shaped Dielecric Elastomer Films

Providing adequate preconditioning prior to their use, for the purpose of actuator design, the mechanical response of conically shaped EDFs (alike those based on the VHB-4905 elastomer) can be represented by hyperelastic models that capture their stabilized equilibrium behavior only. Of course, for DE actuator dynamic analysis and control, these reduced hyperelastic models have to be complemented (for instance, according to the procedure described by Bergstrom and Boyce [33] and as accomplished by Plante [34], [35]) with additional components that capture the inelastic part of the material response which is due to primary viscous effects such as strain-rate-dependent hardening, hysteresis, stress relaxation, and creep. Similar model extensions are also required if temperature-dependent effects (alike the Gough–Joule effect as well as other dissipative, damage, and healing phenomena) or if secondary long-term relaxation effects (such as environment-dependent deterioration of the elastomer molecular structure) are of relevant interest.

A coupled electrohyperelastic boundary value problem based on one algebraic and two ordinary differential nonlinear equations was presented in [36] and adopted for the study of conically shaped EDFs (a similar method was proposed in [37] and applied for studying the out-of-plane electrically induced deformation of inflated planar circular membranes). The model presented in [36] requires a numerical solution routine and is rather uncomfortable for the purpose of actuator design. Here, an alternative model is presented which is simpler but nonetheless enables fast and accurate representation of the FL curves of conically shaped EDFs. This simplified model is based on the assumption that the incompressible EDF is a right circular conical horn with constant wall thickness in any of its deformed configurations (whereas, in reality, it is a general circular conical horn with variable wall thickness as it is assumed both in [36] and in the finite-element calculations that will be reported in the following). The electromechanical force $F_f(V,x)$ that an external user must exert to balance the EDF internal reaction force can be split as

$$F_f(V,x) = {}^{\mathrm{el}}F_f(x) + {}^{\mathrm{em}}F_f(V,x) \tag{3}$$

where

$${}^{\mathrm{el}}F_f(x) = dW/dx \qquad {}^{\mathrm{em}}F_f(V,x) = -dU/dx \tag{4}$$

are elastic and electric conservative force contributions, W and U being the elastic and electric energies stored in the EDF. The electric conservative force ${}^{\mathrm{em}}F_f(V,x)$ will be also referred to as actuation force. Owing to the incompressibility, small relative thickness (with respect to other dimensions and effective radii of curvature), and large prestretches of the employed EDFs, from a macroscopic point of view (i.e., only the practical FL curves of the EDF are of concern rather than the true EDF stress–strain state), it can be assumed that the EDF deforms such that its middle surface coincides with the right circular conical surface spanning the specimen (actuator) rigid disk and ring (as drawn in all reported CAD models, in particular, Figs. 1(c) and (d) and 5). Then, according to this simplification, the aforementioned potential energies can be written as

$$W = \Psi \xi \nu \tag{5a}$$

$$U = \frac{1}{2}\chi C V^2 \tag{5b}$$

where

$$\nu = \pi(r_M^2 - r_m^2)t_0\, y_0^2/y_1^2 \tag{6a}$$

$$C = \varepsilon A^2/\nu \tag{6b}$$

$$A = \pi(r_M + r_m)\sqrt{x^2 + (r_M - r_m)^2} \tag{6c}$$

$$\Psi = \frac{1}{2}\sum_{i=1}^{3} C_i(\lambda_1^2 + \lambda_2^2 + \lambda_1^{-2}\lambda_2^{-2} - 3)^i \tag{6d}$$

$$\lambda_2 = y_1/y_0\lambda_r \tag{6e}$$

$$\lambda_1 = \lambda_2\sqrt{1 + x^2/(r_M - r_m)^2} \tag{6f}$$

ν and C being the volume and the capacitance of the EDF; A, λ_1, and λ_2 being the area and the longitudinal and latitudinal stretches of the simplified EDF middle surface; λ_r and ε being the residual strain and the dielectric permittivity of the acrylic DE material; C_i $(i = 1, 2, 3)$ being the constitutive parameters of the Yeoh-type hyperelastic strain-energy-density function Ψ [38]; while χ and ξ are dimensionless correction factors. From (3)–(6f), the film force contributions take the expressions

$${}^{\mathrm{el}}F_f(l) = \xi\nu\left[\sum_{i=1}^{3} iC_i(\lambda_1^2 + \lambda_2^2 + \lambda_1^{-2}\lambda_2^{-2} - 3)^{i-1}\right]\cdot$$
$$\cdot\,(\lambda_1\lambda_2 - \lambda_1^{-3}\lambda_2^{-1})x/[(r_M - r_m))\sqrt{x^2 + (r_M - r_m)^2}] \tag{7a}$$

$${}^{\mathrm{em}}F_f(V,l) = -\chi x\pi^2 V^2(r_M + r_m)^2\varepsilon/\nu \tag{7b}$$

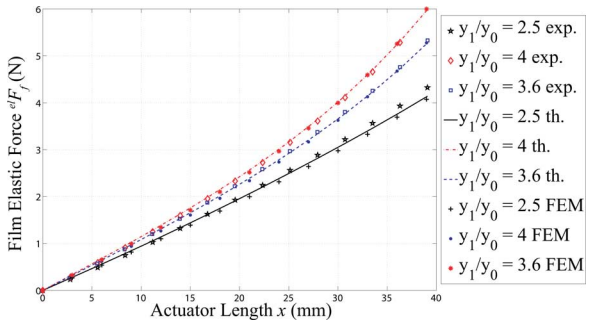

Fig. 10. Elastic conservative force contributions $^{el}F_f$. Comparison between theoretical model (th.), FEM analysis, and experimental (exp.) results.

highlighting that the elastic force can be rather nonlinear in the specimen (actuator) length x, whereas the electric force is linear and quadratic in the specimen (actuator) length x and activation voltage V, respectively. Note that the simplifying geometrical assumption introduced for deriving (13) is as close to reality as the electric potential difference applied between the EDF electrodes is large (for instance, compare Fig. 2(c) and (d) and note that the EDF surface is better approximated to a perfect right circular conical surface when the actuation voltages are larger). Validation of the theoretical curves described by (7a) with the experimental stabilized equilibrium curves is provided in Fig. 10 for three acrylic conically shaped EDFs having identical initial thickness ($t_0 = 1.5$ mm) and internal and external radii (=12 mm and $r_M = 40$ mm) but with different initial film prestretches ($y_1/y_0 = 2.5$, $y_1/y_0 = 3.6$, and $y_1/y_0 = 4$, respectively). Additionally, Fig. 10 also presents the comparison of both theoretical and experimental results with the FL curves obtained via a finite element model (FEM).

The Yeoh constitutive parameters and the residual strain employed in (7a) and in the FEM are $C_1 = 30488$ Pa, $C_2 = 151$ Pa, $C_3 = 8$ Pa, and $\lambda_r = 1.6$. The dimensionless correction factor used in (7a) is $\xi = 0.93$. For the three different initial film prestretches, the experimental stabilized equilibrium curves are found via the apparatus and the procedure that have been employed in the previous section for obtaining Fig. 9. The FEM curves are obtained by solving in FEMLAB (by COMSOL) a large-deformation axial-symmetric model of the experimental specimen, which uses rectangular Lagrange U_2P_1 mixed element type.

Experimental validation at different activation voltages (for V varying between 2 and 7 kV) of the theoretical model described by (7b) is shown in Fig. 11(a), (b), and (c) for acrylic conically shaped EDFs having $y_1/y_0 = 2.5$, $y_1/y_0 = 3.6$, and $y_1/y_0 = 4$, respectively (all featuring $t_0 = 1.5$ mm, $r_m = 12$ mm, and $r_M = 40$ mm). Theoretical curves are obtained for $\varepsilon = \varepsilon_r\varepsilon_0 = 4.5 \times 8.85\text{e}-12\text{F/m}$ and $\chi = 0.6$. For each initial film prestretch, the experimental curves relative to the different activation voltages are generated by subtracting the ON-state- and OFF-state-stabilized equilibrium curves, which have been found via the same apparatus and procedure described in the previous section for obtaining Fig. 9. Figs. 10 and 11 highlight that despite the fact that the middle surface of real conically

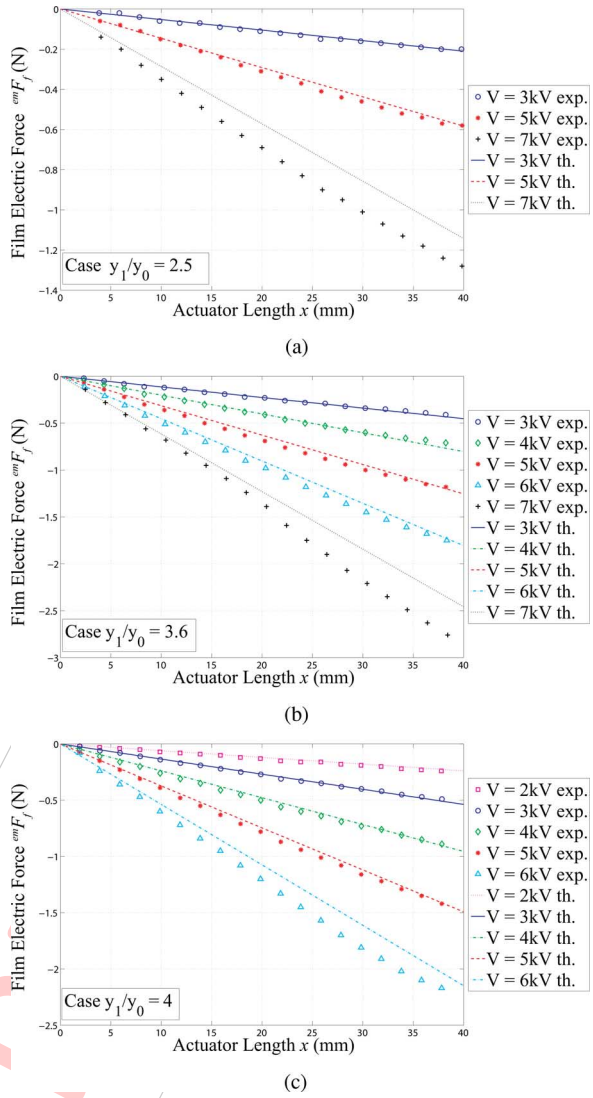

Fig. 11. Electric conservative force contributions $^{em}F_f$. Comparison between theoretical model (th.) and experimental (exp.) results.

shaped EDFs features, in general, a nonzero curvature also in its axial plane [as shown in Fig. 2(c)], the simplified model given by (7) makes it possible to reliably predict the experimental FL curves of practical conically shaped EDFs. The only apparent difference appears in the electric force when the DE is activated at the largest voltages ($V = 7$ kV for the cases $y_1/y_0 = 2.5$ and $y_1/y_0 = 3.6$, and $V = 6$ kV for the case $y_1/y_0 = 4$) which cause significant EDF wrinkling [for instance, see Fig. 8(b)]. This discrepancy, however, is not a serious issue. Indeed, significant wrinkling causes irreversible material damages, such as selective yielding with accompanied loss of pretension, and should be avoided to prevent DE elastic properties to become nonhomogeneous and/or anisotropic. A practical example of a conically shaped EDF that has been irreversibly damaged after significant wrinkling is shown in Fig. 12 in an activated planar configuration. As indicated, in the damaged EDF, two annular subdomains are present: an internal one (where wrinkling occurred and remains), which is softer, and thus, no longer able to

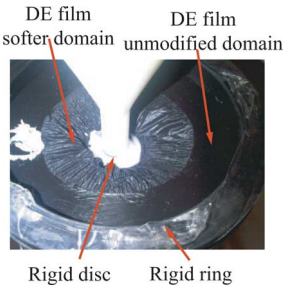

Fig. 12. EDF irreversibly damaged.

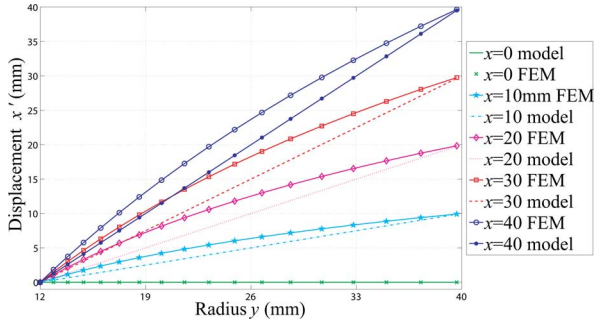

Fig. 13. Comparison between simplified-model and FEM-calculated deformed EDF shapes x'.

stand even modest electric potential differences, and an external one, which maintains the original elastic properties, and thus, is able to stand larger electric potential differences.

Wrinkling is due to the negligible flexural rigidity of EDFs which makes them unable to stand the compressive stresses induced by electrical activation. The necessary and sufficient condition [39] for wrinkling to occur in incompressible elastic EDFs subjected to an electric potential difference V is whenever one of the two principal (longitudinal and latitudinal) elastic Cauchy stresses, ${}^{\mathrm{el}}\sigma_j = \lambda_j \partial\Psi/\partial\lambda_j$ $(j = 1, 2)$, becomes smaller than the electromagnetic Cauchy stress ${}^{\mathrm{em}}\sigma = \varepsilon E^2$, where $E = \lambda_r^2 \lambda_1 \lambda_2 V/t_0$ is the electric field crossing the EDF. By noting that the longitudinal elastic Cauchy principal stress is always larger than the latitudinal one, the theoretical condition for wrinkling to occur is

$$V \geq \frac{t_0 \sqrt{(\lambda_2^2 - \lambda_1^{-2}\lambda_2^{-2}) \sum_{i=1}^{3} i C_i (\lambda_1^2 + \lambda_2^2 + \lambda_1^{-2}\lambda_2^{-2} - 3)^{i-1}}/\varepsilon}{\lambda_r^2 \lambda_1 \lambda_2} \tag{8}$$

which yields $V \approx 6$ kV, $V \approx 4.8$ kV, and $V \approx 4.6$ kV as limiting electric potentials (at $x = 40$mm) for the cases $y_1/y_0 = 2.5$, $y_1/y_0 = 3.6$, and $y_1/y_0 = 4$, respectively. These values are in good agreement with those experimentally measured (i.e., $V = 5.8$ kV, $V = 5.1$ kV, and $V = 4.8$ kV, respectively). Despite the fact that the simplified analytical model given by (7) is capable of capturing the global electromechanical behavior of practical EDFs, caution needs to be exercised instead if local information, such as deformed shape and effective stretches, are required. In particular, local information on effective stretches is important to check for other modes of failure [35] that alike wrinkling may irreversibly compromise actuator functioning. Comparison between simplified model and FEM-calculated deformed shapes x' (axial cross section) and principal stretches of an acrylic conicallyshaped EDF with $y_1/y_0 = 4$ in its OFF-state are reported in Figs. 13 and 14 for x varying between 0 and 40 mm with 10 mm step increment. Note that the shapes of the FEM-calculated principal stretches are in good agreement with those reported in [36].

In particular, Fig. 14(a) and (b) highlights that (6e) and (6f) only provide estimates of the effective EDF principal stretches. However, an FEM analysis campaign enables to find the following analytical relations:

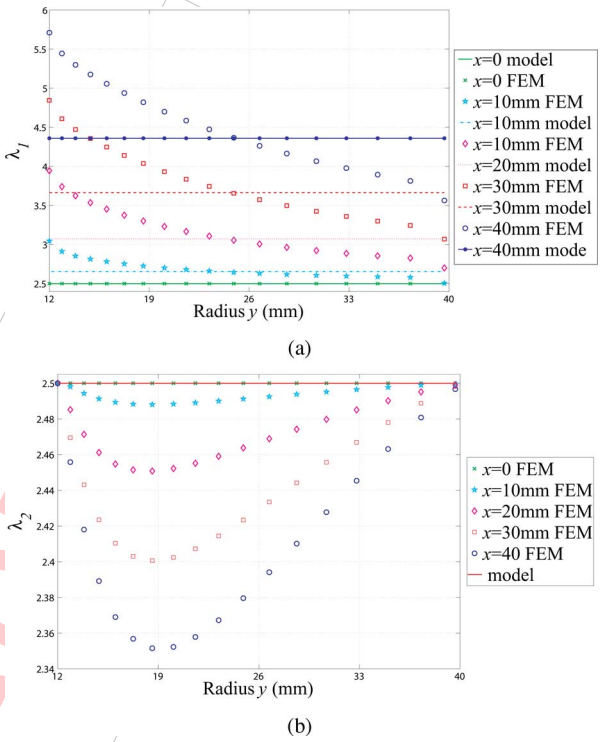

Fig. 14. Comparison between simplified-model and FEM-calculated principal stretches λ_1 and λ_2.

$$\lambda_1^* = \lambda_1 - 0.3 + 70x - 770x^2 \tag{9a}$$

$$\lambda_2^* = \lambda_2 \tag{9b}$$

between the estimates λ_1 and λ_2 given by (6e) and (6f) and the local maximum values λ_1^* and λ_2^* (all the constants in (9a) being expressed in SI units) of the effective longitudinal and latitudinal principal stretches which occur together, for a given x, in the vicinity of the rigid disk as Fig. 14(a) and (b) show. Comparison between (9a) and the FEM analysis is reported in Fig. 15, which highlights excellent agreement irrespective of the initial EDF prestretch y_1/y_0.

This analytical relation is important since, as also indicated in [36], the knowledge of the largest local stretches enables easy check for conditions of mechanical fracture and electric breakdown of conically shaped EDFs.

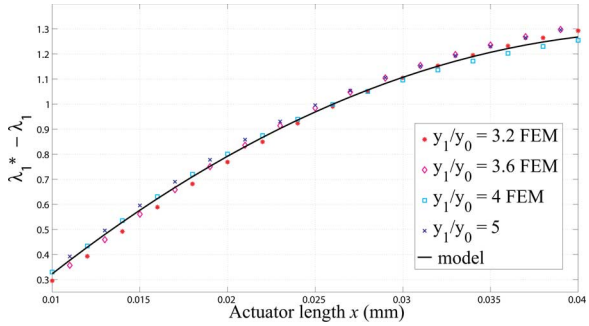

Fig. 15. Comparison between (9a) and FEM analysis.

In particular, practical expressions identifying these conditions of EDF failure are, respectively,

$$\lambda^*_{1\max} \geq \lambda_{\rm br} \tag{10}$$

$$\lambda^*_{1\max}\lambda^*_2\lambda_r^2 V_{\max}/t_0 \geq E_{\rm br} \tag{11}$$

where $\lambda^*_{1\max}$ is the maximum longitudinal stretch value (achieved by λ_1^* when the actuator length x is maximal), $\lambda_{\rm br}$ and $E_{\rm br}$ being the ultimate stretch [40] and the ultimate electric field at break of the employed DE material ($\lambda_{\rm br} = 6$ and $E_{\rm br} =$ 140 MV/m for the VHB-4905). Note that, among all the possible modes of failure, electromechanical instability has not been considered here for conically shaped EDFs since, according to the authors' experience as well as due to the analytical results by others [36], this failure is likely to be less preeminent than mechanical fracture, wrinkling. and electrical breakdown. Besides, it should be noticed that electromechanical instability is the only mode of failure which depends on the employed activation strategy (i.e., a voltage-controlled DE actuator is more prone to electromechanical instability than a charge-controlled one) and on the conceived control scheme (a suitable feedback controller may be devised to stabilize the electromechanically unstable DE actuator).

C. General Remarks on the EDF Models

Let us define x_b and x_f as the initial and final actuator length ($\delta = x_f - x_b$, being the actuator stroke), and the actuation force relative error as $e_T = [\max({}^{\rm em}F_f(x))/\min({}^{\rm em}F_f(x)) - 1]$,[2] where both the maximum and the minimum are evaluated in the range $x_b \leq x \leq x_f$. The actuation force is given by (7b). Considering the EDF parameters as fixed and given a maximum actuation voltage $V_{\max}$, we have

$$e_T = {}^{\rm em}F_f(V_{\max}, x_f)/{}^{\rm em}F_f(V_{\max}, x_b) - 1 = \delta/x_b \tag{12}$$

where it can be seen that the actuation force relative error depends on δ and x_b; in particular, it is null for actuators presenting either a null stroke or large initial actuator length. However, for a given stroke, higher x_b signifies higher actuator dimensions. Note that, a possible way to keep $e_T = 0$ is by adjusting the activation voltage so that

$$V^2 = {}^{\rm em}\overline{F}_f \nu/\chi x\pi^2(r_M + r_m)^2\varepsilon \tag{13}$$

[2]In the following, $\max[f(x)]$ will identify the maximum of $f(x)$ within $x_b \leq x \leq x_f$.

where ${}^{\rm em}\overline{F}_f$ is the desired actuation force.[3] However, in this case, the information about the actual DE position x must be obtained with appropriate sensory systems (or, by using the methods described in [41]) and then fed back to a voltage controller. Obviously, the electric supply should be capable of regulating the voltage.

V. Analytical Model Development for the Slider–Crank-Compliant Mechanism

The FL curve concerning a compliant mechanism can be found by the PRBM using either the principle of virtual work or the free-body diagram approach [30]. Supposing the pin joints being torsional linear springs, the torques due to the deflection of the springs are $T_i = -K_i\Psi_i$, where, with reference to Fig. 6(a), $K_i, i = 1, 2, 3$ are the pivot torsional stiffness to be designed and $\Psi_1 = \vartheta_1 - \vartheta_{10}$, $\Psi_2 = \vartheta_3 - \vartheta_{30} - \vartheta_1 + \vartheta_{10}$, $\Psi_3 = \vartheta_3 - \vartheta_{30}$. The following relationships are found from the position analysis of the mechanism:

$$\vartheta_3 = \pi - \operatorname{asin}\left(\frac{r_1\sin(\vartheta_1) - e}{r_2}\right) \tag{14a}$$

$$x = r_1\cos(\vartheta_1) - r_2\cos(\vartheta_3) \tag{14b}$$

$$\alpha = \operatorname{atan}\left(\frac{e}{x}\right). \tag{14c}$$

Note that, if the compliant mechanism is formed from a monolithic piece, (20) relates ϑ_{30} and ϑ_{10}. From the static analysis of the overall compliant frame having three equal legs, the following FL relationship can be obtained:

$$F_s = 3F_1 + 3F_2 + 3F_3 \tag{15}$$

where

$$F_1 = K_1\Psi_1\cos(\vartheta_3)/r_1\sin(\vartheta_3 - \vartheta_1) \tag{16a}$$

$$F_2 = K_2\Psi_2\cos(\alpha)/r_1\sin(\vartheta_1 - \alpha) \tag{16b}$$

$$F_3 = K_3\Psi_3\cos(\vartheta_1)/x\ \sin(\vartheta_1) - e\ \cos(\vartheta_1). \tag{16c}$$

Let us define the variable $K_{12} = K_1/K_2$ and the function $\Xi = \Xi(K_{12}, r_1, r_2, \theta_{10})$ such that

$$F_{12} = K_1\Xi \tag{17}$$

where

$$\Xi = \frac{\Psi_1\cos(\vartheta_3)}{r_1\sin(\vartheta_3 - \vartheta_1)} + \frac{K_{12}\Psi_2\cos(\alpha)}{r_1\sin(\vartheta_1 - \alpha)}. \tag{18}$$

This expression will be useful when designing the CSCM such that F_{12} is quasi-constant along a given range of motion (see next section).

VI. Design Procedure and Actuator Optimization

A general design methodology is derived which makes it possible to optimize conically shaped dielectric–elastomer linear actuators for known materials and desired force/stroke requirements.

[3]In the following, the desired value of $f(x)$ will be indicated as $\overline{f}(x)$.

A. Design Variables

The actuator available thrust, F_a, is given by (1). The overall actuator design depends on numerous parameters, some of which are defined by the application requirements whereas some others are left free to the designer.

When a DE material is chosen, the dielectric constant ε, the constants $C_i, (i = 1, 2, 3)$, the electric field at break $E_{\rm br}$, the residual stretch after DE preconditioning λ_r, and the ultimate stretch at break $\lambda_{\rm br}$ are given.

It is supposed that the actuator size, r_M and r_m, is given (as determined by the application requirements) along with the actuator initial and final positions x_b, x_f ($\delta = x_b - x_f$ being the desired actuator stroke).

The designer can specify the thrust profile $\overline{F}_a$ at one given voltage (for instance, $V = 0$ or $V = V_{\max}$ or $V = V_{\max}/\sqrt{2}$). Usually, it is wiser to specify $\overline{F}_a^{\rm OFF} = F_a(x, 0)$, which only depends on the actuator elastic properties since $F_a^{\rm ON}(x, V)$ is controllable to a certain extent by means of the applied voltage. At last, the minimum force difference $\Delta\overline{F}_a$ between $F_a^{\rm OFF}(x_b, 0)$ and $F_a^{\rm ON} = F_a(x_b, V_{\max})$ must be defined. Note that, as long as the frame is a passive elastic element, $\Delta F_a(x, V) = {}^{\rm em}F_f(x, V)$.

Variables that are unknown at this stage are:

1) The initial EDF dimensions y_0, t_0. Due to the production techniques of the DEs (which are either purchased as thin films or obtained by injection molding), it is likely that the film thickness t_0 cannot be chosen at will. However, a stack of insulating films can be used to form a single EDF. Therefore, it will be assumed that $t_0 \in \mathbb{I}$, $\mathbb{I}$ being a given set of integer numbers, whereas y_0 is completely left free to the designer.
2) The EDF prestretch in the radial directions y_1/y_0 and the maximum actuation voltage $V_{\max}$. It should be underlined that prestretch in some direction is necessary for the EDF not to wrinkle under actuation. In addition, prestretch increases the breakdown strength of EDFs, thereby improving actuator performance [3], [35]. At last, the effect of prestretch is to alter the EDF dimensions making it thinner and wider, and therefore, increasing ${}^{\rm em}F_f(x, V_{\max})$ (see (6a)–(7b)). Therefore, prestretch should be kept as high as possible.
3) Concerning the CSCM used to correct the actuator stiffness, every kinematic and structural variable is still unknown.

In summary:

1) *Given data*:
   a) **Material properties**.
      i) DE mechanical properties: $C_i, (i = 1, 2, 3)$;
      ii) DE stretch at break: $\lambda_{\rm br}$;
      iii) Residual stretch after DE preconditioning: λ_r;
      iv) DE dielectric constant: ε;
      v) Electric field at break: $E_{\rm br}$;
   b) **Application requirements**.
      i) Actuator dimensions $r_M = y_1$ and r_m;
      ii) Actuator initial and final position (and desired stroke): x_b, x_f;
      iii) Desired thrust profile at a given voltage: $\overline{F}_a$
      iv) Desired actuation force: $\Delta\overline{F}_a = {}^{\rm em}\overline{F}_f$ at $x = x_b$.
2) *Design variables*:
   a) **EDF parameters.**
      i) EDF initial dimensions: y_0, t_0, where $t_0 \in \mathbb{I}$;
      ii) Amount of prestretch: y_1/y_0;
      iii) Maximum actuation voltage: $V_{\max}$.
   b) **Frame parameters.**
      i) Links length and dimensions: r_1, r_2;
      ii) Flexural pivot dimensions: K_i, $i = 1, 3$ and θ_{10}.

B. Design Procedure

The design procedure comprises two steps: first, the determination of the EDF geometrical parameters, and, second, the design of the flexible frame.

1) **Determination of the EDF geometrical parameters**

a) Given a suitable safety factor ϕ_λ to avoid mechanical break, using (6e), (6f), and (9), find the initial EDF dimensions, y_0 (and thus, prestretch, y_1/y_0)

$$\lambda^*_{1\max} = \phi_\lambda \lambda_{\rm br} \Rightarrow$$
$$y_0 = \frac{y_1\sqrt{1 + x_f^2/(r_M - r_m)^2}}{\lambda_r(0.3 - 70x_f + 770x_f^2 + \phi_\lambda\lambda_{\rm br})}. \quad (19)$$

b) Given y_0, using (8), find the electric field at wrinkling, E_w

$$E_w = \sqrt{(\lambda_2^2 - \lambda_1^{-2}\lambda_2^{-2})\sum_{i=1}^{3} iC_i(\lambda_1^2 + \lambda_2^2 + \lambda_1^{-2}\lambda_2^{-2} - 3)^{i-1}\Big/\varepsilon} \quad (20)$$

the stretch λ_1 being evaluated at the position $x = x_f$. Given a suitable safety factor to avoid electrical break $\phi_{\rm el}$, define the limiting electric field E_l as the minimum value between E_w and $\phi_{\rm el}E_{\rm br}$.

c) Given E_l and the desired actuation force $\Delta\overline{F}_a$, using (6a), (6e), (6f), and (7b), find the EDF initial thickness t_0

$$t_0 = \frac{\Delta\overline{F}_a[(r_M - r_m)^2 + {x_f}^2]{y_1}^2}{\chi x_b \pi\varepsilon {E_l}^2({r_M}^2 - {r_m}^2){y_0}^2}. \quad (21)$$

Choose ${t_0}^* \in \mathbb{I}$ such that ${t_0}^* \geq t_0$.

d) Given ${t_0}^*$, the maximum actuation voltage is

$$V_{\max} = E_l {t_0}^*/\lambda_1\lambda_2\lambda_r^2 \quad (22)$$

the stretch λ_1 being evaluated at the position $x = x_f$.

2) **Design of the flexible frame**

a) Impose the UEP at a point $\overline{x}$ such that $x_b \leq \overline{x} \leq x_f$. The imposition of the UEP at a given $\overline{x}$ constrains the dimension of either r_1 or r_2, for instance

$$r_2 = \sqrt{(r_1 - e)^2 + \overline{x}^2}. \quad (23)$$

b) Considering (23), the frame force due to the torsional springs K_1, K_2 is given by

$$F_{1,2} = K_1\Xi(K_{12}, r_1, \theta_{10}). \quad (24)$$

Use multivariable optimization [30] to find K_{12}, r_1, θ_{10} which minimize:

$$\mathfrak{I} = \max \Xi / \min \Xi \tag{25}$$

subject to

$$K_{12} \geq 0; \quad 0 < r_1 < r_M; \quad \theta_{10}^{\min} \leq \theta_{10} \leq \theta_{10}^{\max}. \tag{26}$$

The variable K_{12} and the connecting rod length r_1 are constrained to be positive, $r_{1\max} = r_M$ being imposed by the application constraints. At last, θ_{10} is allowed to vary in the range $[\theta_{10}^{\min}, \theta_{10}^{\max}]$ only, in order to avoid excessive deflections of the elastic joints.

c) Given the desired thrust profile $\overline{F}_a^{\mathrm{OFF}}$ and $\overline{F}_f^{\mathrm{OFF}}(\overline{x})$, find K_1 such that

$$F_{1,2} + \overline{F}_f^{\mathrm{OFF}}(\overline{x}) \approx 0. \tag{27}$$

Given K_{12} and K_1, then $K_2 = K_{12} K_1$.

d) Given the desired frame stiffness $\overline{K}_s$ (e.g., $\overline{K}_s = -K_f^{\mathrm{OFF}}$), find K_3 such that

$$dF_3/dx + \overline{K}_s \approx 0. \tag{28}$$

e) Given the values of K_i, $i = 1, 2, 3$, the designer can find the flexure dimensions. Supposing, for instance, the flexures are straight beam hinges with rectangular cross section, then $K_i = \frac{Y I_{a_i}}{L_i}$, where Y is the frame material Young modulus, L_i is the length of the small-length flexural pivot, and $I_{a_i} = \frac{{h_i}^3 b_i}{12}$ is the moment of inertia of the pivot cross-sectional area with respect to the axis a_i (h_i and b_i denotes the pivot thickness and width, respectively, whereas a_i is the barycentric axis parallel to the width direction).

VII. Case Studies

A. Single-Acting Constant-Force Actuator

The objective of the present case study is to design a single-acting constant force actuator (Case 1, Section II).

1) *Given data*:
   a) **Material properties**:
   C_1 =30 488 Pa, C_2 =151 Pa, C_3 = 8 Pa, $\lambda_{\mathrm{br}} = 6$, $\lambda_r = 1.6$, $\phi_\lambda = 0.8$, ε = 4.5 8.85e-12 F/m, $E_{\mathrm{br}} = 140\,\mathrm{MV/m}$, $\phi_{\mathrm{el}} = 0.9$;
   b) **Application requirements and Circuitry parameters**:
   $y_1 = 40\,\mathrm{mm}, x_b = 20\,\mathrm{mm}, x_f = 30\,\mathrm{mm}, \overline{F}_a^{\mathrm{OFF}} = 0\,\mathrm{N}, \Delta\overline{F}_a = 0.8\,\mathrm{N}$;
2) *Design variables*:
   a) impose $e = 28\,\mathrm{mm}$, $\overline{x} = x_b$
   b) **EDF parameters**:
   $y_0 = 9.9\,\mathrm{mm} \approx 10\,\mathrm{mm}$, $y_1/y_0 = 4$, $t_0 = 1.5\,\mathrm{mm}$, $V_{\max} = 5.1\,\mathrm{kV}$
   c) **Frame parameters.**:
   $r_1 = 20.9\,\mathrm{mm}$, $r_2 = 21.2$, $e = 28\,\mathrm{mm}$, $\theta_{10} = 42°$
   $K_1 = 0.0095\,\mathrm{N{\cdot}m/rad}$, $K_2 = 0.006\,\mathrm{N{\cdot}m/rad}$, $K_3 = 0.047\,\mathrm{N{\cdot}m/rad}$.

Fig. 16(a) shows the EDF FL profile and the moduli of the forces F_1, F_2, and F_3 [as calculated via (15)] in order

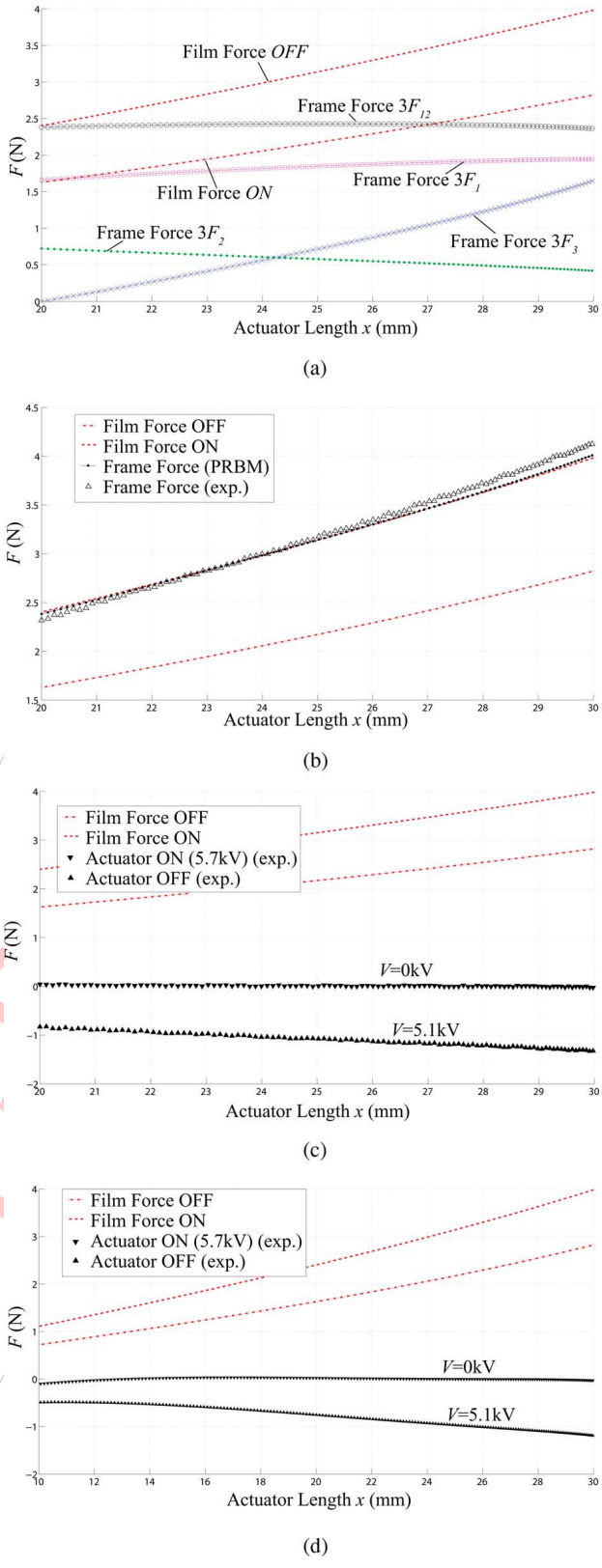

Fig. 16. Single-acting constant-force actuator. Characteristic plots. (a) FL relationship showing the film force F_f and the contribution of forces F_1, F_2, F_3 (shown in moduli) on the overall frame force F_s (found via PRBM). (b) FL relationship showing film force F_f and frame force modulus $|F_s|$ (PRBM and experimental). (c) EDF FL relationship and overall actuator FL relationship. Stroke $x_f - x_b = 10$ mm. (d) EDF FL relationship and overall actuator FL relationship. Stroke $x_f - x_b = 20$ mm.

TABLE I
FLEXURE DIMENSIONS

Dimension	b_i (mm)	h_i (mm)	L_i (mm)
Joint K_1	4	0.07	2.2
Joint K_2	4	0.07	3.4
Joint K_3	4	0.12	2.2

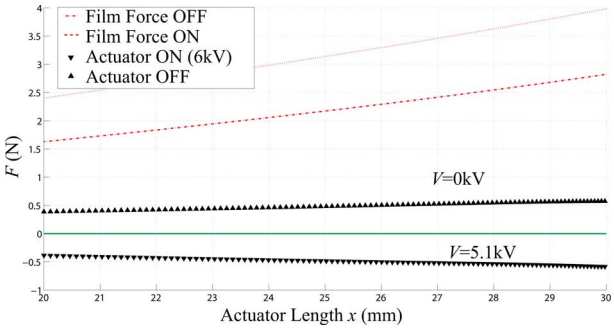

Fig. 17. EDF FL relationship and overall actuator FL relationship. Minimum thrust variation (Case 3, Sec. II).

to highlight their contribution to the overall frame force F_s. In Fig. 16(b), the modulus of the frame force $|F_s|$ (found via PRBM) and the stabilized film forces F_f^{ON}, F_f^{OFF} (found by experiments) are plotted as a function of the actuator length x. The frame behavior is as expected: the modulus of the frame force is parallel to the EDF force F_f^{OFF} for a relevant part of the stroke and it coincides with F_f^{OFF} at $x = \bar{x}$. Concerning the frame material, it must be mentioned that the achievement of high strains without overcoming the material yield strength S_y requires a material with a high S_y/Y ratio [30].

Selecting *Sandvik 11R15* ($Y = 180\,000$ MPa, yield strength 69 MPa) as the flexure material and shaping the hinges as simple leaf springs, obtained from steel sheets of the desired thickness, led to flexure dimensions as reported in Table I.

The frame response has been experimentally evaluated (starting from a single leg) using the test setup shown in Fig. 8(c). As depicted in Fig. 16(b), the experimental results show good agreement with the behavior predicted by the PRBM. Fig. 16(c) shows the experimental overall actuator available thrust F_a. The actuator thrust in the OFF-state is approximately constant (about 0 N) over the range 20–30 mm (in this range, a maximal deviation by 0.01 N is admitted) whereas the actuator thrust in the ON-state is a quasi-linear curve. Note that, if a higher maximal deviation is admitted (0.04 N), the actuator stroke can be increased in the range 10–30mm [Fig. 16(d)].

B. Bidirectional Actuator With Minimum Available Thrust Variation

The objective of the present case study is to design an optimal bidirectional actuator (Case 3, Section II). EDF dimensions are the same as in the previous case study. The only parameters that change are $K_1 = 0.0074$ and $K_3 = 0.042$. Fig. 17 shows the theoretical overall actuator available thrust F_a.

VIII. CONCLUSION

A novel procedure for the optimization of conically shaped dielectric–elastomer-based linear actuators has been presented. The actuators are obtained by coupling a conically shaped EDF and a compliant frame. The proposed frame is used to modify the actuator output so as to obtain a desired profile of the actuator available thrust. The procedure makes it possible to design both EDF and frame, and to develop improved actuators with desired force/stroke requirements. Two case studies have been presented and validated by simulations and experimental results.

REFERENCES

[1] R. Pelrine, R. Kornbluh, and G. Kofod, "High-strain actuator materials based on dielectric elastomers," *Adv. Mater.*, vol. 12, no. 16, pp. 1223–1225, 2000.
[2] R. Pelrine, R. Kornbluh, Q. Pei, and J. Joseph, "High-speed electrically actuated elastomers with strain greater than 100%," *Science*, vol. 287, no. 5454, pp. 836–839, 2000.
[3] G. Kofod, P. Sommer-Larsen, R. Kornbluh, and R. Pelrine, "Actuation response of polyacrylate dielectric elastomers," *J. Intell. Mater. Syst. Struc.*, vol. 14, pp. 787–793, 2003.
[4] F. Carpi, D. D. Rossi, R. Kornbluh, R. Pelrine, and P. Sommer-Larsen, *Dielectric Elastomers as Electromechanical Transducers*. Amsterdam, The Netherlands: Elsevier., 2008.
[5] Q. Pei, R. Pelrine, R. Kornbluh, S. Stanford, N. Bonwit, and J. Heim, "Rolled electroactive polymers," U.S. Patent 6,891,317, 2005.
[6] J. Heim, "High-speed acrylic electroactive polymer transducers," International Patent WO2007/097763, 2007.
[7] S. Dubowsky, M. Hafez, M. Lichter, P. Weiss, and A. Wingert, "Dielectric elastomer actuated systems and methods," U.S. Patent 7,411,331, 2008.
[8] R. Kornbluh, R. Pelrine, J. Eckerle, and J. Joseph, "Electrostrictive polymer artificial muscle actuators," in *Proc. IEEE ICRA Int. Conf. Robo. Auto.*, 1998, vol. 3, pp. 2147–2154.
[9] R. Pelrine and R. Kornbluh, "Electroactive polymer devices," U.S. Patent 6,545,384, 2003.
[10] Q. Pei, M. Rosenthal, S. Stanford, H. Prahlad, and R. Pelrine, "Multiple-degrees-of-freedom electroelastomer roll actuators," *Smart Mater. Struc.*, vol. 13, pp. 86–92, 2004.
[11] A. Wingert, M. D. Lichter, and S. Dubowsky, "On the design of large degree-of-freedom digital mechatronic devices based on bistable dielectric elastomer actuators," *IEEE/ASME Trans. Mechatronics*, vol. 11, no. 4, pp. 448–456, Aug. 2006.
[12] G. Kofod, W. Wirges, M. Paajanen, and S. Bauer, "Energy minimization for self-organized structure formation and actuation," *Appl. Phy. Lett.*, vol. 90, pp. 081916-1–081916-3, 2007.
[13] G. Berselli, R. Vertechy, G. Vassura, and V. Parenti Castelli, "A compound-structure frame for improving the performance of a dielectric elastomer actuator," *Advances in Robot Kinematics*. Berlin, Germany: Springer, 2008, vol. 11, pp. 391–398.
[14] G. Berselli, R. Vertechy, G. Vassura, and V. Parenti Castelli, "Design of a single-acting constant-force actuator based on dielectric elastomers," *J. Mech. Robot.*, vol. 1, no. 3, pp. 031–038, 2009.
[15] G. Berselli, R. Vertechy, G. Vassura, and V. Parenti Castelli, "On designing compliant actuators based on dielectric elastomers for robotic applications," *Robot Manipulators New Achievements*, A. Lazinica and H. Kawai, Eds. InTech, 2010, pp. 523–550. [Online]. Available: http://www.intechopen.com/articles/show/title/on-designing-compliant-actuators-based-on-dielectric-elastomers-for-robotic-applications.
[16] J. E. Huber, N. A. Fleck, and M. Ashby, "The selection of mechanical actuators based on performance indices," *Proc. R. Soc. Lond. A*, vol. 453, pp. 2185–2205, 1997.
[17] D. Nahar and T. Sugar, "Compliant constant-force mechanism with a variable output for micro/macro applications," in *Proc. IEEE ICRA Int. Conf. Robot. Autom.*, vol. 1, pp. 318–323, Sep. 2003.
[18] C. B. W. Pedersen, N. A. Fleck, and G. K. Ananthasuresh, "Design of a compliant mechanism to modify an actuator characteristic to deliver a constant output force," *J. Mech. Des.*, vol. 128, no. 5, pp. 1101–1112, 2006.
[19] R. H. Nathan, "A constant force generation mechanism," *J. Mech. Transm. Auto. Des., Trans. ASME*, vol. 107, pp. 508–512, 1985.

[20] D. Bossert, U. L. Ly, and J. Vagners, "Experimental evaluation of a hybrid position and force surface following algorithm for unknown surfaces," in *Proc. IEEE ICRA Int. Conf. Robot. Autom.*, 1996, vol. 3, pp. 2252–2257.
[21] L. H. Chang and L. C. Fu, "Nonlinear adaptive control of a flexible manipulator for automated deburring," in Proc. *IEEE ICRA Int. Conf. Robot. Autom.*, vol. 4, pp. 2844–2849, 1997.
[22] J. Vogan, "Development of dielectric elastomer actuators for MRI devices," Master's thesis., Dept. Mech. Eng., Massachusetts. Inst. Technol., Cambridge, MA, 2004.
[23] R. Vertechy, G. Berselli, G. Vassura, and V. Parenti Castelli, "Optimal design of lozenge-shaped dielectric elastomer linear actuators: Mathematical procedure and experimental validation," *J. Intell. Mater. Syst. Struc.*, vol. 21, no. 5, pp. 503–515, 2010.
[24] L. Kim and S. Tadokoro, *Electroactive Polymers for Robotic Applications*. Berlin, Germany: Springer., 2007.
[25] Y. Bar-Cohen, *Electroactive Polymer (EAP) Actuators as Artificial Muscles: Reality Potential and Challenges*. Bellingham, WA: SPIE Press, 2001.
[26] J. Plante and S. Dubowsky, "The calibration of a parallel manipulator with binary actuation," *Adv. in Robot Kinemat.*. vol. 11, pp. 291–299, 2008.
[27] C. Bolzmacher, M. Hafez, M. B. Khoudja, P. Bernardoni, and S. Dubowsky, "Polymer based actuators for virtual reality devices and rehabilitation applications," in *Proc. SPIE*, 2004, vol. 5385, pp. 281–289.
[28] G. Berselli, R. Vertechy, G. Vassura, and V. Parenti Castelli, "Experimental evaluation of optimal conically-shaped dielectric elastomer linear actuators," in *Proc. IEEE/RSJ IROS 2009 Int. Conf. Intell. Robo. Syst.*, St. Luis, MO, 2009, pp.2910–2915.
[29] H. Wang and J. Zhu, "Implementation and simulation of a cone dielectric elastomer actuator," in *Proc. SPIE*, 2008, vol. 7266, no. 1, pp. 726607-1–726607-7.
[30] L. Howell, *Compliant Mechanisms*. New York: Wiley, 2001.
[31] B. Jensen and L. Howell, "Bistable configurations of compliant mechanisms modeled using four links and translational joints," *ASME J. Mech. Des.*, vol. 126, pp. 657–666, 2004.
[32] B. L. Weight, "Development and design of constant-force mechanisms," Master's thesis., Dept. Mech. Eng. Brigham Young Univ., 2001.
[33] J. Bergström, M. Boyce, "Constitutive modeling of the large strain time-dependant behavior of elastomers," *J. Mech. Phy. Solids*, vol. 46, pp. 931–954, 1998.
[34] J. S. Plante, "Dielectric elastomer actuators for binary robotics and mechatronics," Ph.D. dissertation, Dept. Mech. Eng., Massachusetts Inst. Technol., Cambridge, MA, 2006.
[35] J. S. Plante and S. Dubowsky, "Large-scale failure modes of dielectric elastomer actuators," *Int. J. Solids Struct.*, vol. 43, pp. 7727–7751, 2006.
[36] T. He, X. Zhao, and Z. Suo, "Equilibrium and stability of dielectric elastomer membranes undergoing inhomogeneous deformation," *J. Appl. Phy.*, vol. 106, pp. 083522-1–083522-7, 2009..
[37] N. Goulbourne, E. Mockensturm, and M. Frecker, "Electro-elastomers: Large deformation analysis of silicone membranes," *Int. J. Solids Struct.*, vol. 44, no. 9, pp. 2609–2626, 2007.
[38] O. H. Yeoh, "Characterization of elastic properties of carbon-black-filled rubber vulcanizates," *Rubber Chem. Technol.*, vol. 63, pp. 792–805, 1990.
[39] D. G. Roddeman, J. Drukker, C. W. J. Oomens, and J. D. Janssen, "The wrinkling of thin membranes: Part i—theory," *J. Appl. Mech.*, vol. 54, no. 4, pp. 884–887, 1987.
[40] S. Kawabata, "Fracture and mechanical behavior of rubberlike polymers under finite deformation in biaxial stress field," *J. Macromol. Sci. Phy.. B*, vol. 8, no. 3–4, pp. 605–630, 1973.
[41] K. Jung, K. J. Kima, and H. R. Choi, "A self-sensing dielectric elastomer actuator.," *Sens. Actuators A*, vol. 143, pp. 343–351, 2008.

Giovanni Berselli received the Laurea degree (*cum laude*) in mechanical engineering from the University of Modena, Modena, Italy, and the Ph.D. degree in mechanics of machines from the University of Bologna, Bologna, Italy, in 2004 and 2009, respectively.

He is currently a Contract Professor at DIEM, Mechanical Engineering Department, University of Bologna. He was a Research Assistant in the Department of Mechanical Engineering, Monash University, Melbourne, Australia, and with CEIT, Escuela Superior de Ingenieros de la Universidad de Navarra, San Sebastian, Spain. His research interests include the design of compliant mechanisms, dexterous robotic hands, compliant actuators based on dielectric elastomers, and infinitely variable transmissions.

Rocco Vertechy received the Laurea degree in mechanical engineering and the Ph.D. degree in mechanics of machines from the University of Bologna, Bologna, Italy, in 2001 and 2005, respectively.

He is currently an Assistant Professor in the Perceptual Robotics Laboratory, Scuola Superiore Sant'Anna, Pisa, Italy. He was a Research Assistant in the Department of Mechanical Engineering, University of Canterbury, Christchurch, New Zealand, and a Visiting Researcher in the Robotics Locomotion Laboratory, Stanford University, Stanford, CA. He was engaged in research on the kinetostatic analysis and synthesis of parallel manipulators. His current research interests include the design and control of robotic systems which physically interact with both humans and unknown constrained environments, as well as of solid-state mechatronic devices which are safe, affordable, and disposable.

Gabriele Vassura received the Laurea degree (*cum laude*) in mechanical engineering from the University of Bologna, Bologna, Italy, in 1972.

He is currently an Associate Professor at DIEM, Mechanical Engineering Department, University of Bologna. His teaching activity is in the field of machine design, mainly focused on mechanical design of automatic machines and robots. His main interests in research are the design of dexterous robotic hands, simulation of pneumatic actuation systems, and design methodologies for automated systems.

Vincenzo Parenti-Castelli received the Laurea degree (*cum laude*) in mechanical engineering from the University of Bologna, Bologna, Italy.

He has been a Full Professor of mechanics of machines at DIEM, University of Bologna, since 1989. He has authored or coauthored more than 200 papers on the following topics: gas lubrication of journal bearings, methods of machine design, fault diagnosis and monitoring of gears, automated systems for milking machines, and robotics. In recent years, his major research interest has been the kinematic and dynamic analysis of open and closed kinematic chains and on biomechanics. He received several awards including the National Federation of the Knights of Work in 1975, and several scholarships including a Fulbright in 1982 and CNR in 1983. He was a Co-Editor of the International Conference Proceedings on Advances in Robot Kinematics in 1992 and 1996 and of Romansy 2010. Since 1994, he has been a Coordinator of the Ph.D Student Committee in Mechanics of Machines at the University of Bologna and a Member of the Editorial Board of the international journal *Meccanica*. Since 2004, he has been Editor-in-Chief of *Meccanica*, and an Associate Editor of *Mechanism and Machine Theory* and a member of the Lombardo Institute—Academy of Sciences and Literature. Since 1995, he has been a member of the Technical Committee on Robots and Manipulators of the International Federation for the Promotion of Mechanisms and Machine Science (IFToMM), Chair of the Permanent Commission on Publications of IFToMM during 2001–2009, and Chairman of the IFToMM–Italy Committee (2009–2011). Since 2002, he has been an Associate Member of the Jozef Stefan Institute of Lubljana.